J Mater Sci: Mater Electron (2017) 28:19010–19016
DOI 10.1007/s10854-017-7855-9

Transparent nano layered Li_3PO_4 coatings on bare and ITO coated glass by thermionic vacuum arc method

Suat Pat[1] · H. Hakan Yudar[1] · Şadan Korkmaz[1] · Soner Özen[1] · Reza Mohammadigharehbagh[1] · Zerrin Pat[2]

Received: 3 July 2017 / Accepted: 1 September 2017 / Published online: 5 September 2017

Abstract In this paper, Li_3PO_4 (LPO) thin films were coated onto bare and indium tin oxide (ITO) coated glass substrates by thermionic vacuum arc technique. The structural, surface, and optical properties of the LPO films were investigated. The properties of the deposited films were analyzed using an X-ray diffraction, field emission scanning electron microscopy, atomic force microscopy, UV–Vis spectrophotometer, and interferometer tools. The miller indices of the crystalline planes of the ITO coated samples were determined as to be (222), (123), (400), (420), (440), (622), and (444). The (200), (121), (112), (301), and (410) miller indices for the crystalline planes were detected for the LPO layers deposited directly on glass. The grain sizes, the microstrain, the lattice strain values, the dislocation density and the number of crystallite per unit area were estimated for LPO layer. The transparency values of the produced Li_3PO_4/glass (sample *S1*) and Li_3PO_4/ITO/glass (sample *S2*) structures were relatively high 87 and 90% for bare and ITO coated glass substrate, respectively. The reflection values of the coated samples onto bare and ITO coated glass were approximately as 0.05 and 0.06 at 550 nm, respectively.

1 Introduction

Lithium ion batteries (LiB) have more advantageous for many reasons. These are excellent shelf life, good power density, flat discharge characteristics, high voltages, and high energy densities [1–3]. Many type LiBs are manufactured according to the technological applications. An all-solid-state battery is a type of the LIBs. An all-solid-state battery consists solid layers including anode, cathode and electrolyte layers. Solid electrolyte layer plays an important role in the battery performance [4]. Solid electrolyte must have only ionic conductivity. Moreover, the solid-state electrolyte is widely used in novel electronic devices and sensors. Thin films should be deposited onto transparent substrates for the all-transparent electronic devices. For the transparent electronic devices, solid electrolyte layers must be deposited on the transparent conductive oxide layers such as indium tin oxide (ITO) layer.

The Li_3PO_4 (LPO) film is used an all-solid electrolyte layer. LPO is a well-known and most used oxide electrolyte material. Also, this layer is a good separator in the rechargeable battery. The all-solid state electrolyte layer is a key material. LPO have only ionic conductivity. It is a chemically stable and safe material [5, 6]. The ideal solid electrolyte should have a high ionic conductivity with a combination of transport numbers and should be stable over a wide potential range of 0–5 V in contact with metallic lithium [7, 8]. The solid electrolyte for LiBs has the features such as nano-structured composites, high power density, long cycle life, high-rate capability, high performance, thermal stability, smaller dimension and excellent safety [9–15].

The LPO thin film as a solid electrolyte layer can key materials for the fully solid-state electronic materials and devices such as microelectronics, communications, smart cards, medical devices, CMOS-based integrated circuit applications, gas sensors, and battery of electric vehicles [16–21].

The LPO films can be deposited by the various methods. These methods are radio frequency magnetron sputtering

✉ Suat Pat
suatpat@ogu.edu.tr

[1] Physics Department, Eskişehir Osmangazi University, Eskişehir, Turkey

[2] Chemistry Department, Bilecik Seyh Edebali University, Bilecik, Turkey

(RF) [22], chemical precipitation [23], spray coating [24], wet chemical [25], thermal evaporation [17], pulsed laser deposition [26], electrostatic spray deposition [27], co-precipitation reaction [28], solid-state reaction [29], ArF excimer laser deposition [30] and etc.

In this study, the LPO thin films were deposited onto the bare and ITO coated glass substrate by the thermionic vacuum arc (TVA) technique, for the first time. TVA is a rapid deposition technology [31–33]. According to other deposition technologies, the films can deposit in shortest time in the high vacuum conditions and low deposition temperatures. So, deposited layers have different properties such as nano structured, low roughness, high adherence, deposition with high ion energy and etc. The effect of the structural, surface and optical properties of coated the LPO thin films on the different substrates were investigated. The annealing process was not performed. The deposition and analysis were realized at room temperature. An UV–Vis spectrophotometer was used to determine the optical properties. The coated samples were investigated by field emission scanning electron microscopy (FESEM) and atomic force microscopy (AFM). X-ray diffraction (XRD) analysis is also used. UV–Vis spectrophotometers (UNICO 4802 double beam) were used for the optical properties of the produced the LPO thin films.

2 Experimental

The surfaces of bare and ITO coated glasses were cleaned by de-ionized water. TVA system was used for the LPO thin film deposition. The TVA is a pure plasma generator and thin film deposition system. TVA system has two electrodes. One of the electrodes is an electron gun and other is a crucible for material deposition. The LPO pieces were placed in the molybdenum crucible. The distance of the between crucible and substrates positions was adjusted to 80 mm. The TVA system works under high vacuum conditions. In this deposition process, the electron gun is used to evaporate of the material placed into the crucible. The electron gun in TVA runs with a direct current. Emitted electrons from the electron gun are accelerated by the DC high voltage power supply to the anode from the electron gun. When the plasma is ignited, the applied voltage is suddenly decreased. In that time, the discharge current is directly increased. The film thickness can be controlled in the TVA system. The electrical parameters of the TVA discharge were kept the same for the depositions. In this paper, two type substrate materials were used. Finally two-type stack formations were manufactured such as Li_3PO_4/glass and Li_3PO_4/ITO/glass structure, named as sample *S1* and sample *S2*, respectively. All thin films were coated at room temperature.

Only one surface of the substrates was used for the coating process. Prior to the start of the coating process, the chamber was vacuumed up to 1.10^{-5} torr. TVA parameters are the filament current (18 A), applied voltage (250 V), drop voltage (100 V), deposition pressure (1.10^{-4} torr), discharge current (0.2 A), and deposition time (25 s). No heat treatment was applied to the substrate before and after the experiment.

A Zeiss SUPRA 40 VP FESEM was used in the analyses of the surface morphology of the produced LPO thin films. Rigaku MiniFlex 600 XRD smart lab goniometer tool was used to measure X-ray pattern of the LPO layers. The surface roughness of samples has been examined by an Ambios Q-Scope AFM. The AFM images of the film surface have been taken by non-contact mode using the Scan Atomic V 5.1.0 SPM control software. UV–Vis spectrophotometer (UNICO 4802 double beam) was used to determine the optical properties of the produced LPO thin films. Filmetrics F20 interferometer tool was used to measurement of the reflectance spectrum of coated LPO layers.

3 Results and discussion

FESEM image of the samples are indicated in Fig. 1. The high-resolution 2D surface imaging and grain dimension were determinate with FESEM. The measurements were realized at higher magnifications. The image in Fig. 1 reveals the granular structure and uniform distribution of spherical particles on the surface of the deposited films. The images of the LPO coated onto bare and ITO coated glass substrates are shown in Fig. 1a, b. The smallest grains were detected on the LPO coated bare glass substrate surface. Surfaces images are not similar. Especially sample *S2* has some cracks. This is a proper property for the ion trapping and Li mass transfer.

The XRD measurements are shown in Fig. 2. XRD patterns were obtained in the range of 20°–70°. Figure 2a, b shows the XRD pattern of LPO coated onto bare and ITO coated glass substrate. The miller indices for the LPO coatings were detected at (200), (121), (112), (301) and (410). These results are good agreement with related literature values [34, 35]. Figure 2b have also different reflection planes of (202), (222), (123), (400), (420), (440), (622) and (444), these reflections planes are related with the ITO substrate [36–38]. Debye–Scherrer formula is seen in the Eq. 1, is used for the calculate of the grain sizes [39]. According to obtained results, microstructural properties of the *S1* and *S2* samples are very close to each other, but grain size of the sample *S2* is smaller than the values of the *S1* sample.

$$D = \frac{K\lambda}{\beta cos\theta} \quad (1)$$

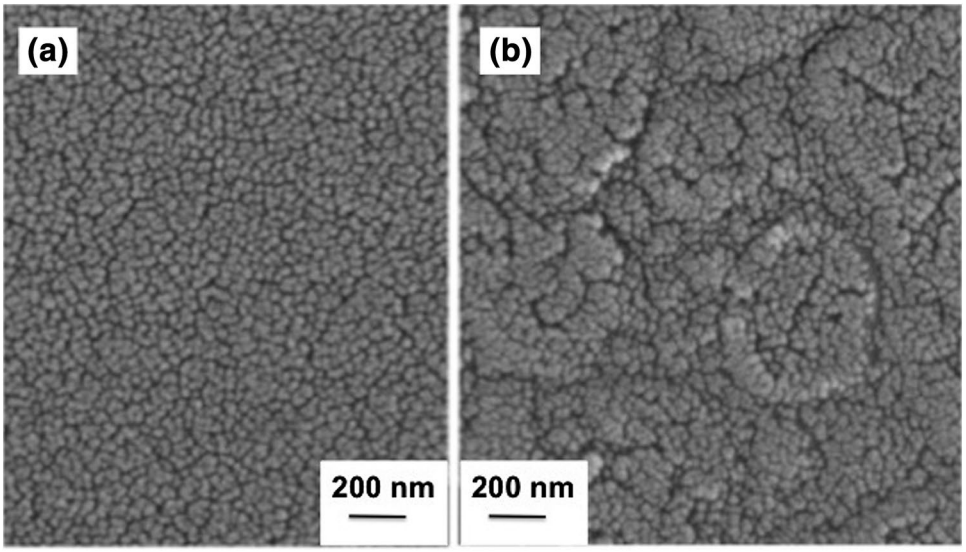

Fig. 1 FESEM images for LPO thin films onto **a** bare and **b** ITO coated glass substrates

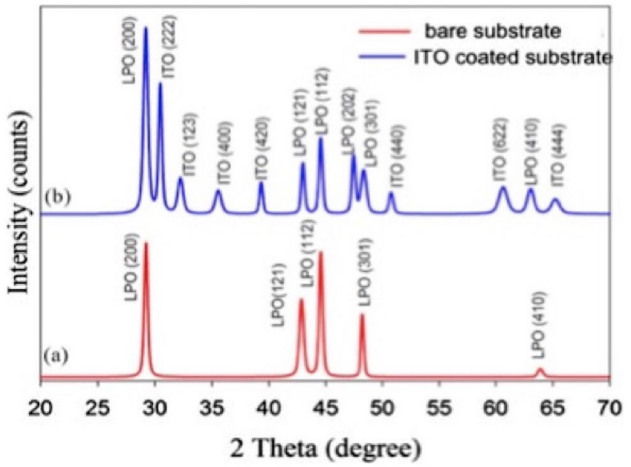

Fig. 2 XRD patterns of LPO coated onto *a* bare and *b* ITO coated glass substrate

where *D, K*, λ, β, and θ symbols are the grain size, shape factor (0.94), used wavelength (1.5406 Å), the full width at half maximum (FWHM) of the observed peak, respectively. Equations 2 and 3 were used to calculate the microstrain and lattice strain of the deposited layers [40, 41].

$$MS = \frac{(\beta \cos \theta)}{4} \tag{2}$$

$$LS = \frac{\beta}{4 \tan \theta} \tag{3}$$

where, *MS* and *LS* are microstrain and lattice strain of the peak. The Eqs. 4 and 5 are used to find the dislocation density and the number of crystallites per unit area.

Table 1 XRD parameters of produced samples *S1* and *S2* sample

Samples	D (nm)	LS	MS	δ (nm^{-2})	N (nm^{-2})
S1	23	0.0060	0.0015	0.0019	0.0080
	19	0.0052	0.0019	0.0028	0.0152
	24	0.0039	0.0015	0.0017	0.0072
	28	0.0031	0.0013	0.0013	0.0047
	20	0.0035	0.0018	0.0027	0.0142
S2	18	0.0078	0.0019	0.0030	0.0134
	22	0.0062	0.0016	0.0021	0.0077
	15	0.0087	0.0024	0.0046	0.0251
	13	0.0087	0.0026	0.0056	0.0339
	24	0.0044	0.0015	0.0018	0.0060
	24	0.0040	0.0015	0.0017	0.0056
	23	0.0041	0.0015	0.0018	0.0065
	22	0.0039	0.0016	0.0019	0.0069
	15	0.0058	0.0024	0.0045	0.0240
	19	0.0043	0.0018	0.0027	0.0110
	11	0.0065	0.0033	0.0087	0.0652
	14	0.0049	0.0026	0.0052	0.0303
	17	0.0062	0.0033	0.0088	0.0660

$$\delta = \frac{1}{D^2} \tag{4}$$

$$N = \frac{t}{D^3} \tag{5}$$

where, δ and *N* are the dislocation density and number of crystallites per unit, respectively [37]. The thicknesses of the films (t) were measured 100 and 80 for sample *S1* and *S2* by Filmetrics F20 thin film measurement system, respectively. The values found using by the equations are given in Table 1.

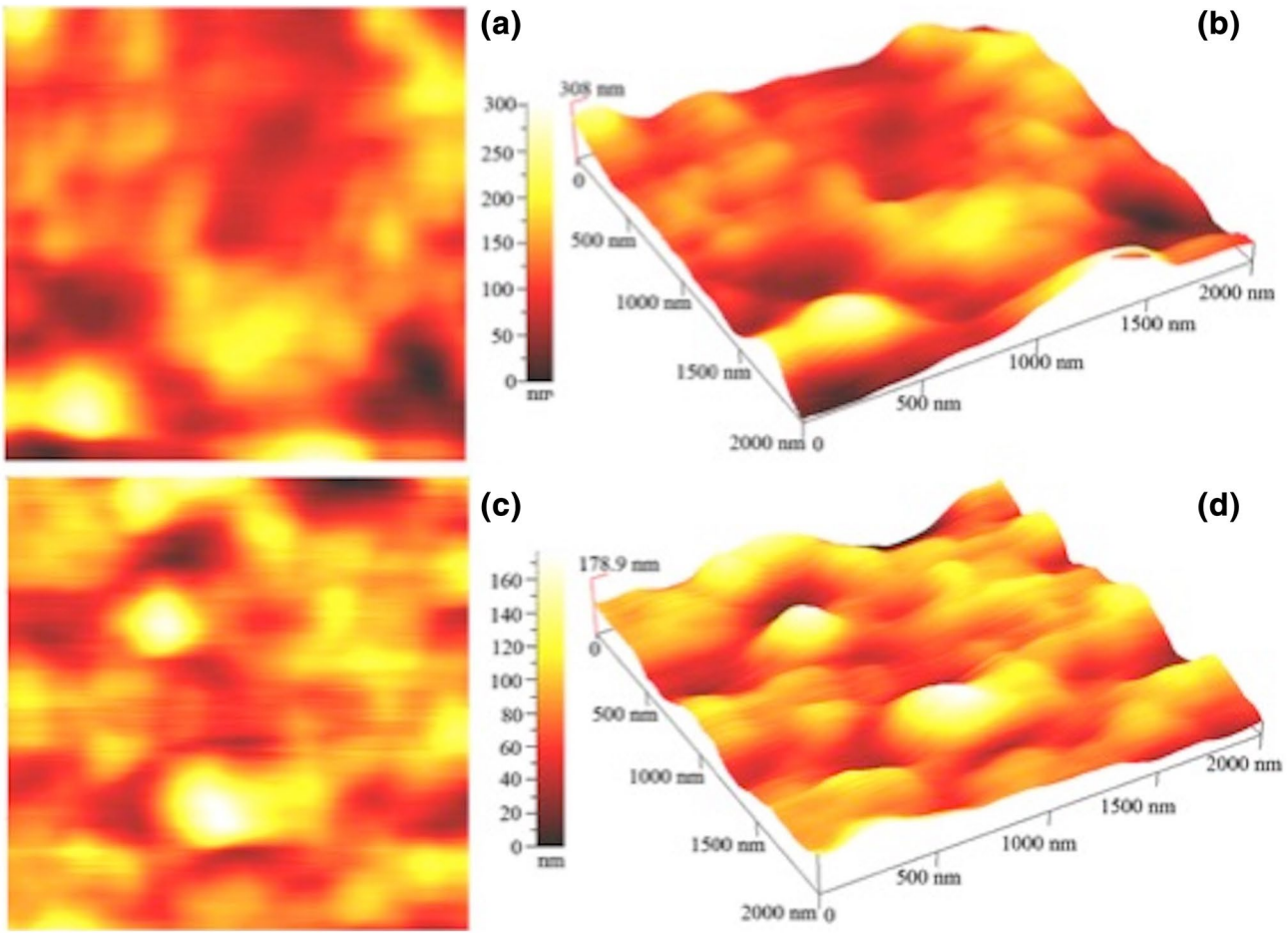

Fig. 3 AFM images of the LPO coated samples. **a** 2D and **b** 3D images for the bare glass, **c** 2D and **d** 3D images for ITO coated glass

Table 2 Surface characterization results of the bare and ITO coated glass substrate

Samples	RMS (nm)	Skewness	Kurtosis
S1	44.8	0.3	0.5
S2	25.7	0.2	0.6

The two-dimensional (2D) and three-dimensional (3D) AFM images of the film surfaces are presented in Fig. 3. These images have obtained in 2 μm × 2 μm scan areas. The 2D images of sample *S1* and *S2* are shown in Fig. 3a, c. The 3D images of the samples are shown in Fig. 3b, d, respectively. The scan angle and rates of the films were 0° and 2 Hz, respectively. The films were growth in island type, relatively.

Root mean square (RMS), Skewness (Ssk) and Kurtosis (Skr) parameters give the characterization results of the coated surface. For the values of these parameters, the measurements were taken at different areas of the films at room temperature and atmospheric pressure. These parameters are shown in the Table 2. According to the values in Table 2, the RMS roughness of the films is increased from 44.8 to 25.7 nm for the sample *S2* the ITO coated substrate. The roughness value for sample *S2* is nearly half of the sample *S1* value.

The absorbance and the transmittance spectra of the deposited layers are shown in Fig. 4. The measurements were realized in the range of 200 and 1000 nm. The absorbance graph is shown in Fig. 4a. Absorbance values are approximately 0.04 or 0.05 for the sample *S1* or *S2*, respectively. The transmittance graph is shown in Fig. 4b. The measured transmittance values are 90 and 87% for *S1* and *S2* samples, respectively. These values were measured at 550 nm. According to Fig. 4, LPO coated onto substrates has been different optical properties. The transmittance value of LPO coated onto ITO glass is respectively low according to the other sample at visible range. It was concluded that the samples have good optical quality due to high transparency and low absorption losses of the films. Figure 5 is shown reflectance spectrum of the LPO. The reflectance values of the samples were found approximately as 0.05 and 0.06 at

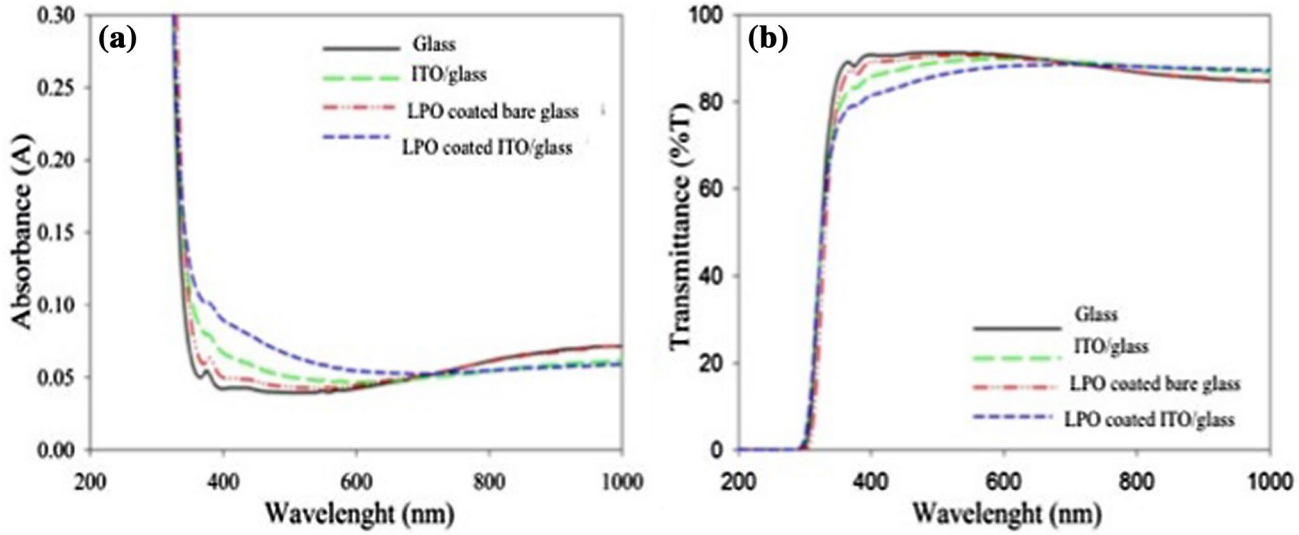

Fig. 4 **a** Absorbance and **b** transmittance spectra of the LPO coated onto bare and ITO coated glass substrates

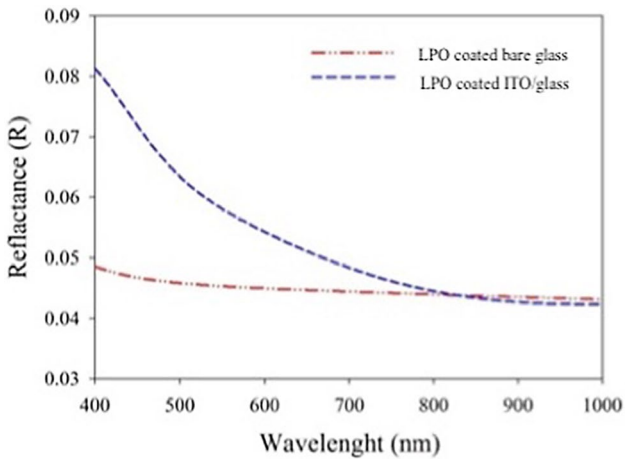

Fig. 5 Reflectance of the LPO coated onto bare and ITO coated glass substrates

550 nm for the sample *S1* and *S2*, respectively. The reflectance of the LPO is different. This difference is also supported by FESEM and AFM images. As these results, the reflectance of the LPO coated ITO glass is more than the value of the LPO coated onto the bare glass substrate.

In this study, the surface, microstructural, optical properties are varied from the substrate effect. Although ITO layer is in the polycrystal form, obtained results are similar to each other and literatures values. The all deposited layers have high transparency values. Finally, it is concluded that TVA is a proper and very fast deposition technology for the LPO thin films layers according to investigated properties.

4 Conclusions

In this paper, LPO layers were coated onto bare and ITO coated substrates by TVA technique without any annealing process. The advantage of TVA method are listed such as more efficiently, higher quality, high uniformity, in a shorter deposition time and etc. All measurements were realized in room temperature. The structural, optical and surface properties of coated LPO samples were investigated using by variously analysis tools. The coated LPO samples thickness had approximately 100 and 80 nm for a bare and ITO coated glass substrates, respectively. The AFM and the FESEM images show that deposited layers are compact, crystalline, and homogeneous. The RMS roughness, the Skewness and the Kurtosis values of the coated samples are different. LPO and ITO reflections planes were detected by X-ray diffractometer. The absorbance, transmittance and reflectance graphs versus wavelength of LPO thin films were obtained. It is seen that the films have different optical properties and these films are transparent. According to results, TVA is a proper deposition technology for LPO coatings.

Acknowledgements This research activity was supported by TUBITAK (Grant No. 115E331).

References

1. H. Li, Z. Wang, L. Chen, X. Huang, Research on advanced materials for Li-ion batteries. Adv. Mater. **21**, 4593–4607 (2009)
2. J. Clement, Investigation of thin film materials for next generation lithium ion batteries (2016)

3. N. Kuwata, S. Kudo, Y. Matsuda, J. Kawamura, Fabrication of thin-film lithium batteries with 5-V-class $LiCoMnO_4$ cathodes. Solid State Ion. **262**, 165–169 (2014)
4. S. Xiong, K. Xie, E. Blomberg, P. Jacobsson, A. Matic, Analysis of the solid electrolyte interphase formed with an ionic liquid electrolyte for lithium-sulfur batteries. J. Power Sources **252**, 150–155 (2014)
5. S.S. Zhang, Liquid electrolyte lithium/sulfur battery: fundamental chemistry, problems, and solutions. J. Power Sources **231**, 153–162 (2013)
6. J. Li, C. Ma, M. Chi, C. Liang, N.J. Dudney, Solid electrolyte: the key for high-voltage lithium batteries. Adv. Energy Mater. (2015). doi:10.1002/aenm.201401408
7. P. Sivakumar, P.K. Nayak, B. Markovsky, D. Aurbach, A. Gedanken, Sonochemical synthesis of $LiNi_{0.5}Mn_{1.5}O_4$ and its electrochemical performance as a cathode material for 5V Li-ion batteries. Ultrason Sonochem **26**, 332–339 (2015)
8. T. Hwang, J. Lee, H. Noh, J. Lee, J. Mun, J.-K. Lee, W. Choi, Surface coating of 5V spinel $LiNi_{0.5}Mn_{1.5}O_4$ cathodes by carbon materials for Li-ion batteries applications, in *Meeting Abstracts, The Electrochemical Society*, 2015, pp. 553–553
9. C.-F. Sun, J. Hu, P. Wang, X.-Y. Cheng, S.B. Lee, Y. Wang, Li_3PO_4 matrix enables a long cycle life and high energy efficiency bismuth-based battery. Nano Lett. **16**, 5875–5882 (2016)
10. J. Liu, B-doped $Li_3V_2(PO_4)_3$/C cathode material with high rate capability for lithium-ion batteries. Ceram. Int. **43**, 2573–2578 (2017)
11. M. Luo, X. Lin, H. Lan, H. Yu, L. Yan, S. Qian, N. Long, M. Shui, J. Shu, Lithiation-delithiation kinetics of $BaLi_2Ti_6O_{14}$ anode in high-performance secondary Li-ion batteries. J. Electroanal. Chem. **786**, 86–93 (2017)
12. D. Mu, Y. Chen, B. Wu, R. Huang, Y. Jiang, L. Li, F. Wu, Nano-sized $Li_4Ti_5O_{12}$/C anode material with ultrafast charge/discharge capability for lithium ion batteries. J. Alloys Compd. **671**, 157–163 (2016)
13. D. Zhou, Y.B. He, R. Liu, M. Liu, H. Du, B. Li, Q. Cai, Q.H. Yang, F. Kang, In situ synthesis of a hierarchical all-solid-state electrolyte based on nitrile materials for high-performance lithium-ion batteries. Adv. Energy Mater. (2015). doi:10.1002/aenm.201500353
14. P. Hou, L. Zhang, X. Gao, A high-energy, full concentration-gradient cathode material with excellent cycle and thermal stability for lithium ion batteries. J. Mater. Chem. A **2**, 17130–17138 (2014)
15. G. Tan, F. Wu, C. Zhan, J. Wang, D. Mu, J. Lu, K. Amine, Solid-state li-ion batteries using fast, stable, glassy nanocomposite electrolytes for good safety and long cycle-life. Nano Lett. **16**, 1960–1968 (2016)
16. J. Feng, B. Yan, M.O. Lai, L. Li, Design and fabrication of an all-solid-state thin-film Li-Ion microbattery with amorphous TiO2 as the anode. Energy Technol. **2**, 397–400 (2014)
17. H.-K. Lee, N.-J. Choi, S.E. Moon, W.S. Yang, J. Kim, A solid electrolyte potentiometric CO_2 gas sensor composed of lithium phosphate as both the reference and the solid electrolyte materials. J. Korean Phys. Soc. **61**, 938–941 (2012)
18. S. Borhani-Haghighi, C. Khare, R. Trócoli, A. Dushina, M. Kieschnick, F. LaMantia, A. Ludwig, Synthesis of nanostructured $LiMn_2O_4$ thin films by glancing angle deposition for Li-ion battery applications. Nanotechnology **27**, 455402 (2016)
19. M. Laurenti, N. Garino, S. Porro, M. Fontana, C. Gerbaldi, Zinc oxide nanostructures by chemical vapour deposition as anodes for Li-ion batteries. J. Alloys Compd. **640**, 321–326 (2015)
20. I.J. Gordon, S. Grugeon, H. Takenouti, B. Tribollet, M. Armand, C. Davoisne, A. Débart, S. Laruelle, Electrochemical Impedance Spectroscopy response study of a commercial graphite-based negative electrode for Li-ion batteries as function of the cell state of charge and ageing. Electrochim. Acta **223**, 63–73 (2017)
21. H. Wang, Z. Liu, D. Chen, Z. Jiang, A new potentiometric SO_2 sensor based on Li_3PO_4 electrolyte film and its response characteristics. Rev. Sci. Instrum. **86**, 075007 (2015)
22. S. Pat, S. Özen, V. Şenay, Ş. Korkmaz, Optical and surface properties of optically transparent Li_3PO_4 solid electrolyte layer for transparent solid batteries. Scanning. (2015). doi:10.1002/sca.21272
23. S. Zhang, S. Xie, C. Chen, Fabrication and electrical properties of Li_3PO_4-based composite electrolyte films. Mater. Sci. Eng. B **121**, 160–165 (2005)
24. Y. Kobayashi, S. Seki, A. Yamanaka, H. Miyashiro, Y. Mita, T. Iwahori, Development of high-voltage and high-capacity all-solid-state lithium secondary batteries. J. Power Sources **146**, 719–722 (2005)
25. E. Kartini, T.Y.S. Putra, Supardi, W. Honggowranto, T. Umbar, M. Manawan, Neutron study on Li_3PO_4 solid electrolyte prepared by wet chemical reaction. in *Asian oceania conference on neutron scattering (AOCNS)*, Sydney, Australia (2015)
26. Y. Sakurai, A. Sakuda, A. Hayashi, M. Tatsumisago, Coating of Li_4SiO_4-Li_3PO_4 solid electrolyte films on $LiCoO_2$ particles by pulsed laser deposition, in *Meeting Abstracts, The Electrochemical Society*, 2010, pp. 596–596
27. Y. Kobayashi, H. Miyashiro, K. Takei, H. Shigemura, M. Tabuchi, H. Kageyama, T. Iwahori, 5 V class all-solid-state composite lithium battery with Li_3PO_4 coated $LiNi_{0.5}Mn_{1.5}O_4$. J. Electrochem. Soc. **150**, A1577–A1582 (2003)
28. X. Li, R. Yang, B. Cheng, Q. Hao, H. Xu, J. Yang, Y. Qian, Enhanced electrochemical properties of nano-Li_3PO_4 coated on the $LiMn_2O_4$ cathode material for lithium ion battery at 55 C. Mater. Lett. **66**, 168–171 (2012)
29. J. Chong, S. Xun, J. Zhang, X. Song, H. Xie, V. Battaglia, R. Wang, Li_3PO_4-coated $LiNi_{0.5}Mn_{1.5}O_4$: a stable high-voltage cathode material for lithium-ion batteries, Chem.-A Eur. J. **20**, 7479–7485 (2014)
30. N. Kuwata, N. Iwagami, Y. Tanji, Y. Matsuda, J. Kawamura, Characterization of thin-film lithium batteries with stable thin-film Li_3PO_4 solid electrolytes fabricated by ArF excimer laser deposition. J. Electrochem. Soc. **157**, A521–A527 (2010)
31. S. Pat, S. Özen, V. Şenay, Ş. Korkmaz, Z. Pat, Solid state battery manufacturing with thermionic vacuum ARC and RF sputtering. in *2015 IEEE International Conference on Plasma Sciences (ICOPS), IEEE*, 2015, pp. 1–1
32. S. Özen, V. Şenay, S. Pat, Ş. Korkmaz, AlGaAs film growth using thermionic vacuum arc (TVA) and determination of its physical properties. Eur. Phys. J. Plus **130**, 1–6 (2015)
33. S. Özen, V. Şenay, S. Pat, Ş. Korkmaz, The influence of voltage applied between the electrodes on optical and morphological properties of the InGaN thin films grown by thermionic vacuum arc. Scanning. (2015). doi:10.1002/sca.21237
34. C. Keffer, A.D. Mighell, F. Mauer, H.E. Swanson, S. Block, Crystal structure of twinned low-temperature lithium phosphate. Inorg. Chem. **6**, 119–125 (1967)
35. J. Bi, T. Zhang, K. Wang, B. Zhong, G. Luo, Controllable synthesis of Li_3PO_4 hollow nanospheres for the preparation of high performance $LiFePO_4$ cathode material. Particuology **24**, 142–150 (2016)
36. T.O.L. Sunde, E. Garskaite, B. Otter, H.E. Fossheim, R. Sæterli, R. Holmestad, M.-A. Einarsrud, T. Grande, Transparent and conducting ITO thin films by spin coating of an aqueous precursor solution. J. Mater. Chem. **22**, 15740–15749 (2012)
37. H.H. Yudar, Ş. Korkmaz, S. Özen, V. Şenay, S. Pat, Surface and optical properties of indium tin oxide layer deposition by RF magnetron sputtering in argon atmosphere. Appl. Phys. A **122**, 748 (2016)

38. D. Choi, S.-J. Hong, Y. Son, Characteristics of indium tin oxide (ITO) nanoparticles recovered by lift-off method from TFT-LCD panel scraps. Materials **7**, 7662–7669 (2014)
39. H.H. Yudar, S. Pat, Ş. Korkmaz, S. Özen, V. Şenay, Zn/ZnSe thin films deposition by RF magnetron sputtering. J. Mater. Sci, **28**, 1–5 (2016)
40. Ş. Korkmaz, B. Geçici, S.D. Korkmaz, R. Mohammadigharehbagh, S. Pat, S. Özen, V. Şenay, H.H. Yudar, Morphology, composition, structure and optical properties of CuO/Cu_2O thin films prepared by RF sputtering method. Vacuum, **131**, 142–146 (2016)
41. S. Sharma, S. Vyas, C. Periasamy, P. Chakrabarti, Structural and optical characterization of ZnO thin films for optoelectronic device applications by RF sputtering technique. Superlattices Microstruct. **75**, 378–389 (2014)